




Article

Fluorescence In Situ Hybridization-Based Chromosome Aberration Analysis Unveils the Mechanistic Basis for Boron-Neutron Capture Therapy's Radiobiological Effectiveness

Valerio Cosimo Elia ^{1,2,†} , Francesca Fede ^{1,2,†}, Silva Bortolussi ^{3,4} , Laura Cansolino ^{4,5}, Cinzia Ferrari ^{4,5} , Emilia Formicola ², Ian Postuma ⁴ and Lorenzo Manti ^{1,2,*} 

¹ Radiation Biophysics Laboratory, Department of Physics “E. Pancini”, University Federico II, 80126 Naples, Italy; velia@na.infn.it (V.C.E.); francesca.fede@na.infn.it (F.F.)

² Istituto Nazionale di Fisica Nucleare, INFN, Naples Section, 80126 Naples, Italy; eformico@na.infn.it

³ Department of Physics, University of Pavia, 27100 Pavia, Italy; silva.bortolussi@unipv.it

⁴ Istituto Nazionale di Fisica Nucleare, INFN, Pavia Section, 27100 Pavia, Italy; laura.cansolino@unipv.it (L.C.); cinzia.ferrari@unipv.it (C.F.); ian.postuma@pv.infn.it (I.P.)

⁵ Department of Clinical Surgical Sciences, University of Pavia, 27100 Pavia, Italy

* Correspondence: lorenzo.manti@unina.it

† These authors contributed equally to this work.

Abstract: Boron-Neutron Capture Therapy (BNCT) is a tumor-selective radiotherapy, based on the nuclear capture reaction $^{10}\text{B}(n,\alpha)^7\text{Li}$ producing short range α -particles and recoiling ^7Li nuclei exclusively confined to boron-enriched cancer cells. These particles possess high Linear Energy Transfer (LET) and mainly generate clustered DNA strand breaks, which are less faithfully restored by intracellular repair. Mis-rejoined breaks yield chromosome aberrations (CAs), which, for high-LET radiation, are more complex in nature than after sparsely ionizing photons/electrons used in conventional radiotherapy, which leads to increased cell-killing ability. However, such a radiobiological tenet of BNCT has been scantily studied at the DNA level. Therefore, the aim of this work was to evaluate CAs induced by BNCT in comparison to X-rays in genomically stable normal human epithelial mammary MCF10A cells. Two Fluorescence In Situ Hybridization (FISH)-based techniques were applied to calyculin A-induced prematurely condensed chromosomes: Whole Chromosome Painting and multicolor(m)-FISH. Not only did BNCT induce a greater CA frequency than X-ray irradiation, but m-FISH karyotype-wide analysis confirmed that CAs following BNCT exhibited a much higher degree of complexity compared to X-rays. To our knowledge, this is the first time that such evidence supporting the radiobiological superiority of BNCT has been shown.

Keywords: BNCT; BPA; FISH techniques; chromosome aberration; complex DNA damage; high-LET radiation



Citation: Elia, V.C.; Fede, F.; Bortolussi, S.; Cansolino, L.; Ferrari, C.; Formicola, E.; Postuma, I.; Manti, L. Fluorescence In Situ Hybridization-Based Chromosome Aberration Analysis Unveils the Mechanistic Basis for Boron-Neutron Capture Therapy's Radiobiological Effectiveness. *Appl. Sci.* **2024**, *14*, 1171. <https://doi.org/10.3390/app14031171>

Academic Editor: Ioanna Kyriakou

Received: 10 January 2024

Revised: 26 January 2024

Accepted: 29 January 2024

Published: 30 January 2024



Copyright: © 2024 by the authors. Licensee MDPI, Basel, Switzerland. This article is an open access article distributed under the terms and conditions of the Creative Commons Attribution (CC BY) license (<https://creativecommons.org/licenses/by/4.0/>).

1. Introduction

Inasmuch as cancer incidence is growing globally, external beam radiotherapy (RT) remains one of most effective strategies in oncological disease management and cure. Recent years have witnessed remarkable technological advances in RT that have improved the precision of the dose distribution to deep-seated tumors [1]. A clear example is protontherapy, whose physical properties ensure greater sparing of healthy tissue than photon-based conventional radiotherapy (CRT), thus abating the risk of RT-induced secondary cancers [2]—a crucial requirement, especially for pediatric patients [3]. However, this is of little avail against tumor radioresistance. Proton beams used clinically are radiobiologically equivalent to photons, with a slightly higher relative biological effectiveness (RBE) equal only to some 10%.

Aside from high-RBE carbon ion radiotherapy (CIRT), which is still hampered by costs and a lack of robust evidence-based clinical advantages [4], recently proposed physics-based strategies such as Proton-Boron Capture Therapy (PBCT) have been shown to enhance

in vitro proton biological effectiveness [5,6]. However, PBCT conceptually stems from the much longer standing Boron-Neutron Capture Therapy (BNCT) approach, which is based on the well-known nuclear reaction $^{10}\text{B}(n,\alpha)^7\text{Li}$. The rationale of BNCT is that low-energy (0.0025 eV) thermal neutrons interact with ^{10}B incorporated preferentially by tumor cells, leading to the emission of one α -particle (^4He) and one recoiling ^7Li nucleus [7–10]. As these reaction products have a summed range in the order of a cell nucleus diameter ($\sim 10\ \mu\text{m}$), in principle, only cancer cells will incur the damage brought about by the emitted particles [11–13]. Moreover, the high Linear Energy Transfer (LET) possessed by the reaction products is supposed to confer such particles a highly DNA-damaging action. This represents the putative radiobiological cornerstone [14] for the greater effectiveness consistently shown by BNCT both in vitro and in clinical trials. Hence, BNCT may be valuable in overcoming cancer radioresistance [7,9,15–17]. Specifically, Wang et al. recently reviewed the most relevant clinical trials for a variety of disease sites both in terms of boron delivery agents as well as prognosis, spanning from as early as 1951 up to 2019, and reported results that support BNCT is a better overall prospective treatment modality compared to CRT for cancers, such as glioblastoma multiforme, meningiomas, head and neck, lung, sarcomas, melanomas as well as pediatric tumors and metastatic sites, among others [17]. Although radiobiological studies have been carried out [13,16,18], the vast majority are understandably on BNCT-induced loss of tumor clonogenicity and cell death in general [19–21]. Since little has been investigated at the molecular level [20,22,23], the actual mechanisms governing the cellular response to BNCT remain to be elucidated. In fact, as recently reviewed in [24], it has been speculated that the BNCT-mixed fields diminish the ability to repair DNA Double-Strand Breaks (DSBs), the most cytotoxic radiation-induced lesion [25,26], by interfering with DNA Damage Response (DDR) pathways.

High-LET radiation predominantly induces clustered DSBs that are associated with a higher lethality due to their poor reparability [26–28]. As structural chromosome aberrations (CAs) arise from DSB mis-rejoining, a mechanistic link between BNCT-induced cell death and lethal CAs has been long proposed [29] but never substantiated by experimental data. Therefore, in this work, we focused on the measurement of CAs following BNCT as compared to low-LET X-ray irradiations with the specific intent of measuring the level of CA complexity. This is because as the ionization density increases, so does the likelihood that complex-type CAs arise [30–32], these being defined as involving at least two chromosomes, two arms and three breaks [33]. Hence, to ascertain whether the greater ability of the mixed radiation field associated with the BNCT is ascribable to such LET-dependent increase in CA complexity, we used two Fluorescence In Situ Hybridization (FISH) techniques—Whole Chromosome Painting (WCP) and multicolor(m)-FISH. The former paints two pairs of homologous chromosomes and allows rapid quantification of the overall damage burden induced; the latter, instead, adds valuable information specifically on the degree of complexity within the detected spectrum of the aberration types [34–36]. Boronophenylalanine (BPA), an amino acid derivative actively incorporated by cancer cells [8], was used as a boron carrier. The normal immortalized breast epithelial MCF-10A cell line, frequently used in radiobiology to study normal-cell radiation-induced damage and particularly in CA studies due to its stable genome, was the in vitro model system of choice so as to avoid the confoundingly high baseline frequency of inherently genomic unstable cancer cell lines. Using WCP, we found that the presence of BPA enhanced the frequency of CAs in samples exposed to thermal neutrons compared to those observed in cells exposed to X-rays at the same doses. Moreover, m-FISH-based karyotype examination revealed a much higher frequency of complex CAs following BNCT compared to X-ray exposure; in particular, the number of chromosomes and that of breaks involved per complex CA was markedly greater in BNCT-treated samples. We therefore showed for the first time that DNA damage complexity is the key factor for the radiobiological effectiveness of BNCT in keeping with the high-LET components of the radiation field elicited by the neutron capture reaction.

2. Materials and Methods

2.1. Cell Culture Maintenance

Human epithelial mammary MCF10A cells, a gift by Dr. P. Chaudhary, School of Medicine, Dentistry and Biomedical Sciences, Queen's University Belfast, UK, were grown in standard tissue culture T75 flasks in a humidified atmosphere of 5% CO₂ in air at 37 °C. The growth medium consisted of DMEM/F12 containing 5% horse serum, endothelial growth factor (20 ng/mL), hydrocortisone (0.5 mg/mL), insulin (10 mg/mL) and cholera toxin (100 ng/mL). Cells were routinely subcultured by means of concentrated trypsin 10× using serum-enriched (20%) DMEM/12 medium devoid of all supplements for quenching of trypsin and dilutions [37]. Penicillin/streptomycin was added to both media (1%). At 48 h prior to exposure to the various radiation types, cells were seeded at appropriate densities ($\cong 2 \times 10^5$ cells) in T25 flasks so as to have log-phase cultures at the time of irradiation.

2.2. X-Ray Irradiation

X-ray irradiation was carried out using a STABILIPAN 2 (Siemens, Munich, Germany) radiogen machine available at the Radiation Biophysics Laboratory, University of Naples Federico II, Italy. X-rays were produced by a Thomson tube (TR300F, Siemens, Munich Germany) equipped with a tungsten anode at a working maximum voltage of 250 kVp and filtered by 1 mm thick Cu foil. The dose rate was approximately 1.37 Gy min⁻¹ as previously determined with an Accu-Pro Radcal[®] ionization chamber (model 10X6-06, RadCal, Monrovia, CA, USA). Specifically, cells were placed on a plexiglass support at a given distance from the X-ray exit window. Since the ionization chamber is not flat, to have a measurement of the dose rate as accurate as possible at the position where the cells would be, the plexiglass support (Figure 1) was lowered by an amount such that the center of the sensitive volume of the ionization chamber would coincide with the position of the cell monolayer. Therefore, after the dose rate measurement, the support was brought up by that amount and routine irradiations were carried out by setting on the tube control unit at the appropriate time so as to deliver the desired dose. Dose uniformity was consistently within 1% across the 14 × 11 cm² radiation field.

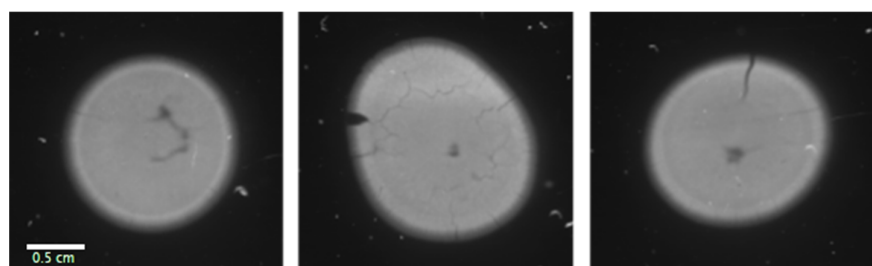


Figure 1. Neutron autoradiography imaging of three representative MCF-10A pellets after BPA treatment. The cell pellets (after washing) were deposited on Mylar disks and irradiated in contact with the sensitive CR-39 detector. The pictures are the results of the chemical etching of the CR-39. The images do not show single tracks on the detector but the distributions of the tracks on the entire sample. The grayscale intensity is representative of the amount of boron in the sample. Lighter areas correspond to higher boron uptake regions. Boron distribution appears homogeneous.

2.3. BPA Preparation and Cell Treatment for BNCT Irradiation

¹⁰B-enriched (~99%) BPA was prepared adding fructose to obtain solubility: a 0.14 M solution was obtained combining BPA (¹⁰B-enriched, L-isomer) with a 10% molar excess of fructose in water. The pH was adjusted to 9.5–10 with NaOH, the mixture was stirred, and after a few minutes, the pH was re-adjusted to 7.4 with HCl.

Before neutron irradiation, the cells were treated for 4 h with BPA previously weighed out and thoroughly dissolved in an appropriate volume of cell growth culture medium. Following filtration by 0.22 μm syringe filters, the working concentration of 80 μg of

^{10}B per mL of culture medium (that is, 80 parts per million, ppm) was achieved corresponding to approximately 1.67 mg/mL of BPA [21]. Subsequently, the BPA-containing medium was removed and, after three washes with PBS (Phosphate-Buffered Saline solution), was replaced with BPA-devoid medium.

2.4. BNCT Irradiation

The cellular samples were irradiated at the TRIGA Mark II research reactor at LENA (Laboratorio di Energia Nucleare Applicata), University of Pavia, Italy. Cells were irradiated in a position of the existing irradiation facility inside the thermal column of the reactor where the thermal neutron flux is about $8 \times 10^7 \text{ cm}^{-2} \text{ s}^{-1}$ at 1 kW, with low epithermal and fast neutron components, as well as low gamma dose [38]. MCF-10A cells were exposed in T25 flasks to 5 kW and 20 kW neutrons for 10 min for each reactor power to yield absorbed doses of 0.5 and 2 Gy, respectively, assuming a boron uptake of 30 ppm. Dosimetry for BNCT experiments consists of calculating by Monte Carlo N-Particle (MCNP6) transport code [38] and the dose deposited in cells by the charged secondary particles set in motion by neutron interaction in cells and in the materials. Neutron flux and spectrum in the cell irradiation position are well known and validated. The calculations were made by projecting the fission neutron source on 6 surfaces surrounding the irradiation position using the SSW/SSR MCNP instructions in order to obtain a better efficiency. A first run was implemented to calculate the reaction rate of neutron captures in boron, nitrogen and hydrogen, to characterize the component of neutron-proton scattering, and to assess the photon dose by electron transport. A second run was carried out by defining a uniform source of protons, alpha particles and ^7Li ions which were transported in the best possible detail to estimate dose. The dose was then normalized using the reaction rate previously calculated and the assumed boron concentration. Specifically, the absorbed dose was calculated considering all the radiation components, as shown in Table 1, of the mixed radiation field of BNCT. This was estimated using a validated TRIGA Mark II reactor model written with MCNP6. Of note, computational dosimetry was obtained by transporting all the secondary particles of the mixed radiation field generated by BNCT in the cell layer, without equilibrium assumptions [39].

Table 1. Dose components for neutron irradiation in the thermal column of the LENA TRIGA Mark II research reactor.

Absorbed Dose [$10^{-6} \text{ Gy s}^{-1} \text{ kW}^{-1}$]			
$^{10}\text{B}(n,\alpha)^7\text{Li}$ per ug/g of ^{10}B	$^{14}\text{N}(n,p)^{14}\text{C}$	H (n,n') H	gamma
5.07 ± 0.01	8.56 ± 0.01	3.02 ± 0.03	17.68 ± 0.03

Verification of Boron Uptake in Cells

The actual boron intracellular uptake was evaluated by neutron autoradiography [40] using Solid-State Nuclear Track Detectors (SSNTDs, Mi.am Srl, Piacenza, Italy), i.e., allyl diglycol carbonate ($\text{C}_{12}\text{H}_{18}\text{O}_7$), known as CR-39 (Columbia Resin) and commonly used for particle beam fluence and retrospective calculations in radiobiology. Neutron autoradiography allows performing imaging of boron distributions. Imaging was obtained for each experiment in samples treated the same day and undergoing the same procedure as the ones irradiated for radiobiological assays. On the day of irradiation, a cellular pellet (consisting of about 4×10^6 cells) was deposited on Mylar films and let dry out for at least 48 h. The films on CR-39 were irradiated at the TRIGA reactor at 20 kW for 30 min, in a position of the facility where the thermal neutron flux is $8 \times 10^6 \text{ cm}^{-2} \text{ s}^{-1}$ at 1 kW. After irradiation, the CR-39 detectors were subjected to chemical etching in a PEW₄₀ ($\text{KOH} + \text{C}_2\text{H}_5\text{OH} + \text{H}_2\text{O}$) basic solution for 10 min at 70 °C to enlarge the diameter of the latent tracks and make them visible under microscope observation. For these experiments, a Leica stereomicroscope (Leica Microsystems Srl, Milan, Italy), provided with an integrated camera connected to a PC was used. The images were acquired and processed with Image Pro Plus 7.0.8.

2.5. Cytogenetic Preparation

Radiation-induced genotoxicity was assessed by measurement of structural CA frequencies in MCF-10A cells following X-ray irradiation or neutron exposure. Scoring of CAs was carried out in chemically induced interphase chromosomes obtained as previously described [41,42]. Briefly, at 24–36 h post-irradiation, cells were incubated for 30 min in the presence of calyculin A (50 ng/mL, (Merck KGaA, Darmstadt, Germany) to induce Premature Chromosome Condensation (PCC). Calyculin-A treated cells were then trypsinized and resuspended in dilution tubes after centrifugation to be subjected to hypotonic treatment (25 min in 75 mM KCl at 37 °C), followed by fixation on ice in freshly prepared Carnoy solution (3:1 *v/v* methanol/glacial acetic acid). Finally, slides were prepared by dropping the solution on pre-warmed (42 °C) wet slides and air-dried at room temperature (RT) for at least 24 h. Slide aging was carried out for a few days at 37 °C prior to chromosome hybridization.

2.6. Chromosome Hybridization

CAs were detected by means of two Fluorescence In Situ Hybridization (FISH)-based techniques: conventional Whole Chromosome Painting (WCP) and the more advanced karyotype-wide multicolor (m)-FISH analysis.

2.6.1. WCP

As previously described [41,43], for WCP, the two pairs of homologous chromosomes 1 and 2 were labeled with probes (MetaSystems ProbesGmbH, Altlussheim, Germany) emitting in the green (chromosome #1, XCP-1 FITC) or red (chromosome #2, XCP-2 orange) spectrum under UV light, respectively. An amount of 8 µL from each probe was aliquoted and used for a 24 × 40 mm² slide area. Chromosome denaturation (72 °C for 3 min) followed by probe hybridization (37 °C for 4 h) was performed using a programmable HYBrite[®] chamber system (ThermoBrite, Abbott, IL, USA). As per the manufacturer's instructions, post-hybridization washes were performed (0.4X SSC or Saline-Sodium Citrate, pH 7.0–7.5, at 72 °C; RT 2X SSC, pH 7.0 containing 0.05% Tween20[®]) and chromosomes were counterstained by 4, 6-diamidino-2-phenylindole (DAPI/antifade, 250 ng/mL).

2.6.2. m-FISH

For m-FISH, all chromosomes were labeled with a finite number of spectrally distinct fluorophores in a combinatorial fashion by means of the 24 X-Cyte (Metasystems, Germany) probe cocktail (CyTM5, DEAC, FITC, Spectrum Orange[™], Texas Red) as described more in detail elsewhere [5,6]. In short, chromosomes and probes were separately denatured. An appropriate amount of the latter was aliquoted in an Eppendorf tube (12 µL for a 24 × 24 mm² coverslip). Slides with PCC spreads were treated sequentially according to the following steps: immersion in 2× SSC solution at 70 °C for 30 min; bathing at RT in 0.1× SSC for 1 min; rinsing in 0.07 NaOH for 1 min at RT; two washes in 0.1× and 2× SSC for 1 min each at 4 °C. Finally, slides were sequentially washed in an ethanol series (70%, 95% and 100%). While slides air-dried, the cocktail probe was denatured by high-temperature (75 °C) incubation in a water bath for 5 min; the probe-containing Eppendorf tube was then rapidly transported on ice to another water bath for incubation at 37 °C for 30 min. The denatured probe was then applied to the slides. PCC spreads were thus hybridized for 48 h using the above-mentioned chamber set at 37 °C. Post-hybridization washing and counterstaining were carried out in the same fashion as described for WCP.

2.7. Scoring and Analysis of CAs

An epi-fluorescence microscope (Axioplan2 imaging MOT, Carl Zeiss AG, Oberkochen, Germany) connected to a computerized platform (Metafer 4, MetaSystems) was used for automated scanning of slides. This allowed digital acquisition of each fluorophore color for subsequent classification of CA rearrangements, either manually by direct observation in the case of WCP or through dedicated software for karyotype reconstruction in the case of m-

FISH-painted PCC spreads. Specifically, CA analysis of WCP-treated samples was carried out by the same scorer on three-color stored images from blind-coded slides. Classification of CAs detected by m-FISH was carried out in accordance with the 24Xyte labeling scheme as provided by the manufacturer after karyotyping of the PCC spreads by the ISIS imaging software, v. 5.2.23 (MetaSystems, Germany), which attributes a false color pattern depending on overlap signals intensity. All types of structural aberrations as originally defined by Savage [44] were scored separately and categorized in simple exchanges (i.e., translocations and dicentrics), either visibly structurally complete or incomplete, acentric excess fragments and complex exchanges, these being assessed as the result of an exchange involving not less than three breaks in at least two chromosomes (that is the Chromosome, Arm, Break criterion—CAB) [33,36]. When more than one option to achieve completeness was possible, the rearrangement that produced the minimum CAB was used. For this study, the frequency “ f ” of all classified CAs was calculated as the ratio between all exchange-type aberrations “ n ” (simple plus complex, both reciprocal and nonreciprocal) and the number of cells scored “ N ”, which was not less than 500 cells for WCP (1500 for unirradiated controls) and at least 100 cells for m-FISH:

$$f = \frac{n}{N} \quad (1)$$

The standard error σ was calculated assuming the frequency f as binomially distributed:

$$\sigma_f = \sqrt{\frac{f*|f-1|}{N}} \quad (2)$$

The same formulas were used for the frequency of complex aberrations alone as well as for the number of chromosomes or of breaks involved in complex exchanges per total number of scored cells as a measure of the degree of complexity in the observed chromosomal rearrangements [5,45]. If necessary, statistical significance was determined at the 95% confidence level by a Two-Sample t -test using SYSTAT (version 13.1, US).

3. Results

3.1. Boron Distribution Imaging

Control samples of MCF-10A cells without boron were measured to check for potential contaminations, i.e., to prove that no boron due to other sources was present, and they in fact did not contain boron. Figure 1 reports pictures of boron distribution imaging for the samples of MCF-10A pellets. The images were obtained by irradiation with high neutron fluence and subsequent etching. The charged particles, generated by neutron interaction in boron, damage the detector along their tracks. The chemical attack of the etching solution enlarges the tracks until they merge, forming a map of boron distribution. The light gray corresponds to the area of the detector where tracks are superposed, obtaining an imaging of the whole cell sample. The distribution is well uniform, demonstrating an even uptake of BPA in the whole cell population, being consistent with the historical experience with cell uptake using BPA with the described protocol. The image of boron distribution is compatible with the assumed boron concentration of 30 ppm, by our previous experience of boron uptake in cell cultures.

3.2. BNCT Is More Effective Than X-rays at Causing DNA Damage

The overall burden of chromosomal damage caused by BNCT is represented in Figure 2. This shows the frequency of all CAs measured in MCF-10A PCC spreads following exposure to X-rays or BNCT at two doses (0.5 and 2 Gy) plus unirradiated controls: at each dose, and for both irradiation modalities, results are presented as obtained by conventional WCP and m-FISH scoring. Data clearly show that treatment by BNCT led to a much greater occurrence of CAs compared to X-rays. Already at the lowest dose used, the CA frequency as assessed by WCP following BNCT was more than 4-fold higher than that found after X-rays (that is, 0.32 ± 0.02 vs. 0.076 ± 0.007). This gap increased with dose as the CA frequency for BNCT at 2 Gy exceeded that caused by the same dose of X-rays by

a factor of more than 7, with about 1.9 aberrations per cell compared to 0.25, respectively (Figure 2). The effectiveness of BNCT at damaging cellular DNA becomes even more evident when CAs were scored by m-FISH, which consistently yielded an absolute value for the CA frequency that was markedly higher than that scored by WCP, demonstrating the ability of m-FISH to identify all structural exchanges involving any chromosome [35,36]. For example, the overall incidence of chromosomal rearrangements was 10-fold higher after BNCT than after X-rays at 2 Gy (8.0 ± 0.8 vs. 0.79 ± 0.04 as shown in Figure 2). No statistically relevant evidence of an increase in overall CA frequency was observed in MCF-10A cells between control samples treated or not with BPA.

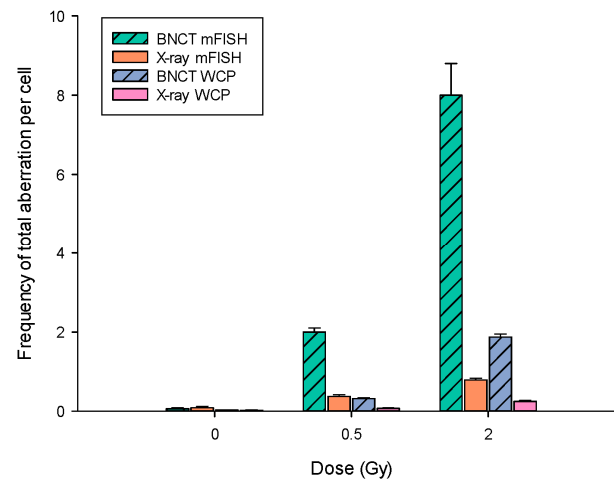


Figure 2. Comparison between the frequency of total aberrations per cell yielded by BNCT (hatched bars) and X-ray irradiation and measured using WCP or m-FISH for the two doses used. Unirradiated controls show similarly low levels of spontaneous CAs.

3.3. BNCT Causes More Complex DNA Damage Than X-rays

Cells irradiated with the neutron thermal flux in the presence of the ^{10}B carrier BPA yielded a significantly higher proportion of complex-type CAs than following X-rays (Figures 3 and 4). Specifically, for X-rays at 0.5 Gy, the occurrence of such aberration type was almost negligible by either technique whereas at the same dose in BNCT-treated samples, analysis by WCP and m-FISH showed frequencies of around 0.08 and 0.25 complex rearrangements per cell, respectively (Figure 3). In the case of m-FISH, the latter value increased to 1.9 ± 0.1 at 2 Gy for BPA-treated samples compared to a complex CA frequency of just 0.08 ± 0.03 for MCF-10 irradiated with X-rays. In particular, the results found for 2 Gy demonstrate well the appropriateness of m-FISH-based karyotype-wide analysis in unveiling the “true” occurrence of radiation-induced DNA complex damage as 2.5-fold more complex-type CAs were found after labeling by m-FISH than after WCP in BNCT-treated samples (hatched vs. plain bars in Figure 3). That the spectrum of measured CAs shifts towards a greater complexity following BNCT than after X-ray irradiation is immediately visible in Figure 4, which shows the relative weight of complex CAs on the overall yield of CAs. An example of the complexity in the spectrum of aberrations that m-FISH can detect is shown in Figure 5, which compares two karyotypes from control and 2 Gy BNCT. These results strongly suggest an effect of the BNCT-associated fusion reaction’s high-LET products [5,28]. As expected, no complex aberrations were found in unirradiated controls.

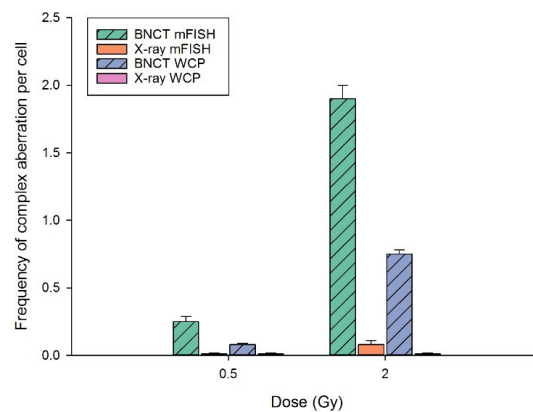


Figure 3. Occurrence of complex aberrations per cell obtained using WCP and m-FISH for the two doses used following BNCT (hatched bars) or X-rays.

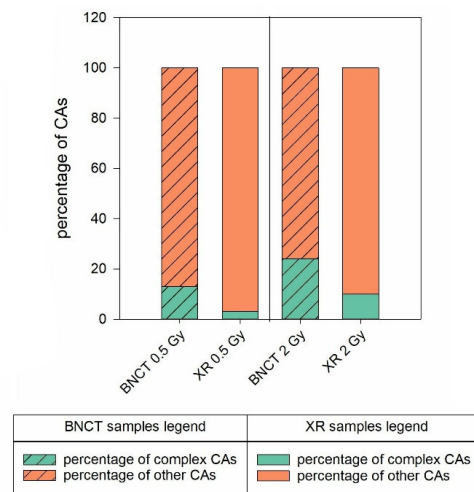


Figure 4. Incidence of complex-type damage following BNCT (hatched bars) or X-rays as obtained using WCP and m-FISH: the two doses that used complex CAs are more frequently observed after BNCT than following X-rays.

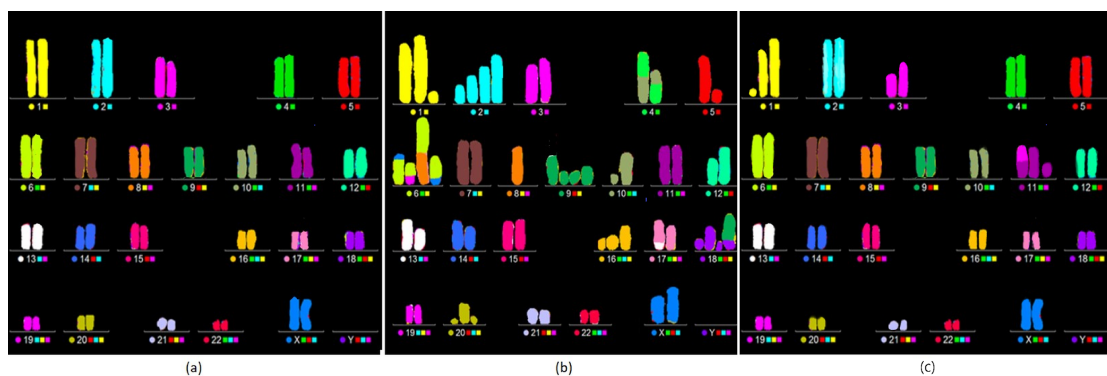


Figure 5. Reconstructed karyotypes by m-FISH from PCC spreads: (a) karyotype from an unirradiated cell; (b) karyotype from a PCC following 2 Gy BNCT. The irradiated cell shows an aberrated karyotype with a significant excess of complex CAs plus other rearrangements, namely, three complex CAs involving chromosomes 10 and 4, another involving chromosomes 9 and 18 (both with 3 breaks), and another involving chromosomes 3, 6, and 8 and X. Additionally, a non-reciprocal translocation between chromosomes 13 and 17, and several fragments from chromosomes 1, 2, 5, 16 and 20 were found; (c) karyotype from a PCC exposed to 2 Gy of X-rays showing a simple exchange (incomplete translocation between chromosomes 3 and 11) and an acentric fragment from one of the two copies of chromosome 1.

BNCT Greatly Enhances the Degree of Complexity Associated with Complex Aberrations Detected by m-FISH

m-FISH analysis allowed us to measure the number of chromosomes and that of breaks involved per complex aberrations normalized by the total number scored. These figures were taken as representing the degree of complexity associated with the treatment with BNCT or X-rays [5]. As clearly shown by Figures 6 and 7, a very marked level of complexity accompanies the complex exchanges found in the BNCT-exposed samples, concurrent with the notion of high LET-induced chromosomal damage, while the much fewer complex CAs observed after X-ray irradiation (Figures 3 and 4) exhibited a minimal number of chromosomes or breaks involved even at the highest X-ray dose, that is 0.19 ± 0.04 and 0.24 ± 0.04 , respectively. By contrast, at 2 Gy, the frequencies of chromosomes per complex exchange per cell and those of breaks per complex exchange per cell were 5.9 ± 0.5 and 7.9 ± 0.7 , respectively, in the case of the BNCT-treated samples.

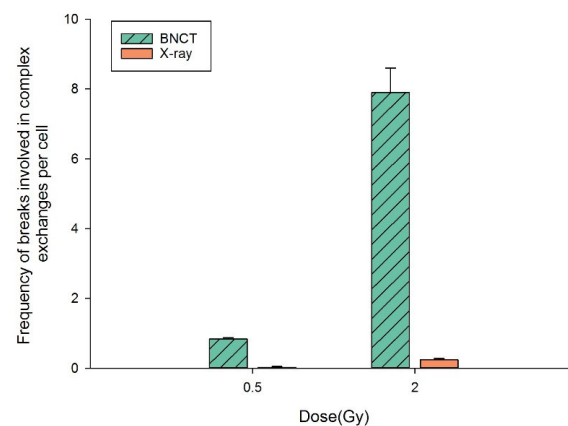


Figure 6. Comparison of the degree of complexity measured in the complex exchanges scored between BNCT- and X-ray-irradiated samples as expressed in terms of the number of chromosomes involved per complex CA.

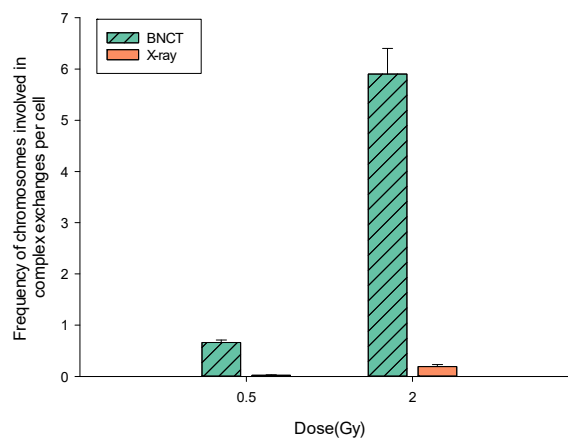


Figure 7. The number of breaks giving rise to the complex exchanges detected by m-FISH in BNCT- and X-ray-irradiated samples confirms the much higher degree of DNA damage complexity elicited by the BNCT-associated $^{10}\text{B}(n,\alpha)^7\text{Li}$ reaction.

4. Discussion

Despite not being yet routinely implemented in clinics worldwide, BNCT has been long advocated as a strategic radiotherapy (RT) modality, particularly against radioresistant tumors, due to its much greater relative biological effectiveness (RBE) compared to conventional RT (CRT) based on low-Linear Energy Transfer (LET) photons and/or electrons [10,17,46–48]. For this reason, we did not perform cellular irradiations in the

absence of the ^{10}B carrier. Indeed, a boost in BNCT-related research and clinical application is occurring nowadays as the development of compact accelerator-based neutron sources paves the way for its in-hospital use, and hence for more advanced clinical trials [12,49]. The potential superiority of BNCT over CRT stems from the radiobiological properties of the high-LET products of the $^{10}\text{B}(\text{n},\alpha)^7\text{Li}$ reaction [13,46]. In fact, while several studies have clearly demonstrated how effectively BNCT impairs the reproductive integrity of cancer cells, as reviewed in [7,16], for example, scant data exist on the BNCT-specific biomolecular mechanisms presiding over such elevated RBE [24,25,50].

It is a long-standing notion that high-LET particles are likely to cause damage sites containing multiple lesions in close spatio-temporal vicinity [28,51]. Such highly clustered lesions, on a nanometer scale, may encompass base damages, Single- and Double-Strand Breaks (SSBs and DSBs, respectively), and challenge the repair capacity of the cells, impacting the major known pathways for restitution of DSBs (the most cytotoxic lesions), i.e., homologous recombination (HR), the classical nonhomologous end-joining (c-NHEJ) and the backup nonhomologous end-joining (b-NHEJ). Specifically, clustered damage repair remains an open question, but recent findings seem to point to alternative NHEJ pathways to participate in the case of highly complex DSBs [26,52] leading to a lower rate of faithful rejoining. This, in turn, is likely to lead to the formation of chromosome aberrations (CAs), with a greater occurrence of complex rearrangements compared to low-LET radiation reflecting the denser ionization pattern of energy deposition events along the tracks [32,53] such as those of the particles emitted in the $^{10}\text{B}(\text{n},\alpha)^7\text{Li}$ reaction. Hence, a causal link between the superiority of BNCT at cell killing and an increased occurrence of lethal aberrations compared to lower LET radiations is likely to exist [29], although this has never been convincingly demonstrated in radiobiological studies thus far.

We therefore investigated the frequency of CAs in BPA-treated cells exposed to a thermal neutron beam by two well-established chromosome labeling techniques, i.e., WCP and m-FISH, and compared the observed frequencies of overall CAs and of complex-type aberrations with those measured following low-LET (X-rays) irradiation. Human mammary epithelial MCF-10A cells were used to avoid the confoundingly high baseline CA frequency from genomically unstable cancer cells. As expected, the overall aberration occurrence was found to increase with dose for both types of irradiations (X-rays and BNCT) as revealed by both techniques (Figure 2). However, BPA-treated samples exposed to BNCT exposure did consistently show a significantly higher frequency of all types of CAs scored by both techniques. More importantly, the marked increase in the frequency of complex-type CAs (Figures 3 and 4) clearly highlights the greater effectiveness of BNCT-associated reaction products at causing complex DNA damage compared to X-rays in agreement with the prevalence of highly clustered damage, whose repair is error-prone [54].

It has also to be noted that our data confirm the underestimation of CA frequency by conventional WCP, which offers the advantage of a rapid assessment of DNA damage as it paints only a limited number of pairs of homologous chromosomes (in our case, chromosomes 1 and 2), compared to the much more expensive and time-consuming m-FISH (Figure 2). This is crucial as far as complex-type aberrations are concerned as they involve more chromosomes simultaneously. In fact, m-FISH allowed us to unveil that radiation-associated complex chromosome damage was of even greater magnitude than inferred by WCP alone in BNCT samples (Figure 3) owing to the scoring of the entire karyotype (Figure 5). Furthermore, m-FISH allowed us to quantify the staggering degree of damage complexity in terms of the mean number of chromosomes (Figure 6) and of breaks (Figure 7) per complex aberration in the BNCT compared to X-ray-irradiated samples. In line with previous work on bimodal therapeutic approaches [5], these data altogether convincingly support the role of the $^{10}\text{B}(\text{n},\alpha)^7\text{Li}$ reaction as the key factor underlying the radiobiological effectiveness of BNCT.

To our knowledge, this is the first study to show that the most likely cause of the therapeutic advantages granted by BNCT is the complexity of the chromosomal damage caused by the BNCT-generated high-LET particles [54]. This damage is prone to misrepair,

thereby increasing cell lethality; work by Schmid et al. [55] has, in fact, shown a greater occurrence of dicentric chromosomes in metaphases from cells subjected to the BNCT mixed radiation field at various doses, including 0.5 and 2 Gy as used in our study, although they report a lower aberration frequency compared to ours. Indeed, scoring of CA in mitotic cells can lead to underestimation in the case of high-LET exposure as the most heavily damaged cells will incur longer cell-cycle delays, which the use of calyculin A-induced Premature Chromosome Condensation (PCC) circumvents [56]. Moreover, it is true that dicentric chromosomes are a well-known lethal aberration as they lead to mitotic failure and their frequency well correlates with loss of clonogenicity [57]. However, dicentric chromosomes, unlike complex-type CAs, are not a specific biomarker of high-LET exposure [36], which our data prove is mechanistically the reason for the therapeutic attractiveness of BNCT.

Overcoming cancer radioresistance remains a priority in any RT scenario and several novel approaches are being explored via the combination of physics- and biology-based strategies [58], natural compound-based radiosensitization [59], or even by entirely new technological advances in hadrontherapy [60]. Our results confirm that BNCT is a truly promising option to treat radioresistant tumors due to the elevated level of poorly repairable damage induced at the DNA level. Together with ongoing studies to identify the most effective routes in boron delivery to improve cancer cell-specific toxicity and the exciting perspectives due to the new generation of accelerator-based neutron production [8,12,61,62], this study may contribute to moving BNCT closer to its adoption in clinical routine in other countries that may thus follow the example recently set by Japan [63].

5. Conclusions

This work represents an *in vitro* radiobiological study on the putative radiobiological mechanisms underlying Boron-Neutron Capture Therapy (BNCT) via the detection and quantification of radiation-induced chromosome aberrations (CAs), which give insights into energy deposition patterns at the DNA level. By employing Fluorescence In Situ Hybridization (FISH) techniques, not only did we find that the overall frequency of CAs was greater in BNCT-treated BPA-containing cells than after X-ray irradiation, but for the first time, we showed that more complex-type CAs were associated with BNCT. Assessment of the elevated degree of complexity in such aberrations allows us to conclude that the therapeutic superiority of BNCT over conventional radiotherapy lies in its capacity to cause extremely clustered, poorly repairable DNA damage.

Author Contributions: Conceptualization, L.M., S.B. and V.C.E.; methodology, C.F., I.P., L.C., L.M. and V.C.E.; software, F.F.; formal analysis, E.F. and F.F.; investigation, C.F., F.F., L.C., L.M. and V.C.E.; resources, C.F., L.M. and S.B.; data curation, F.F., L.M. and V.C.E.; writing—original draft preparation, F.F., L.M. and V.C.E.; writing—review and editing, C.F., F.F., I.P., L.M. and S.B. All authors have read and agreed to the published version of the manuscript.

Funding: INFN funds from National Scientific Committee 5 were received for nuclear reactor fees.

Institutional Review Board Statement: Not applicable.

Informed Consent Statement: Not applicable.

Data Availability Statement: Raw data are not publicly available due to privacy reasons but can be readily provided upon request to the corresponding author.

Acknowledgments: The authors wish to thank personnel at the TRIGA Mark II reactor, University of Pavia.

Conflicts of Interest: The authors declare no conflicts of interest.

References

1. Fiorino, C.; Guckemberger, M.; Schwarz, M.; van der Heide, U.A.; Heijmen, B. Technology-Driven Research for Radiotherapy Innovation. *Mol. Oncol.* **2020**, *14*, 1500–1513. [[CrossRef](#)]
2. Eaton, B.R.; MacDonald, S.M.; Yock, T.I.; Tarbell, N.J. Secondary Malignancy Risk Following Proton Radiation Therapy. *Front. Oncol.* **2015**, *5*, 261. [[CrossRef](#)]

3. Berrington de González, A.; Gibson, T.M.; Lee, C.; Albert, P.S.; Griffin, K.T.; Kitahara, C.M.; Liu, D.; Mille, M.M.; Shin, J.; Bajaj, B.V.M.; et al. The Pediatric Proton and Photon Therapy Comparison Cohort: Study Design for a Multicenter Retrospective Cohort to Investigate Subsequent Cancers After Pediatric Radiation Therapy. *Adv. Radiat. Oncol.* **2023**, *8*, 101273. [[CrossRef](#)]
4. Lazar, A.A.; Schulte, R.; Faddegon, B.; Blakely, E.A.; Roach, M., 3rd. Clinical Trials Involving Carbon-Ion Radiation Therapy and the Path Forward. *Cancer* **2018**, *124*, 4467–4476. [[CrossRef](#)]
5. Bláha, P.; Feoli, C.; Agosteo, S.; Calvaruso, M.; Cammarata, F.P.; Catalano, R.; Ciocca, M.; Cirrone, G.A.P.; Conte, V.; Cuttone, G.; et al. The Proton-Boron Reaction Increases the Radiobiological Effectiveness of Clinical Low- and High-Energy Proton Beams: Novel Experimental Evidence and Perspectives. *Front. Oncol.* **2021**, *11*, 682647. [[CrossRef](#)]
6. Cirrone, G.A.P.; Manti, L.; Margarone, D.; Petringa, G.; Giuffrida, L.; Minopoli, A.; Picciotto, A.; Russo, G.; Cammarata, F.; Pisciotto, P.; et al. First Experimental Proof of Proton Boron Capture Therapy (PBCT) to Enhance Protontherapy Effectiveness. *Sci. Rep.* **2018**, *8*, 1141. [[CrossRef](#)]
7. Barth, R.F.; Zhang, Z.; Liu, T. A Realistic Appraisal of Boron Neutron Capture Therapy as a Cancer Treatment Modality. *Cancer Commun.* **2018**, *38*, 36. [[CrossRef](#)]
8. Barth, R.F.; Mi, P.; Yang, W. Boron Delivery Agents for Neutron Capture Therapy of Cancer. *Cancer Commun.* **2018**, *38*, 35. [[CrossRef](#)]
9. Barth, R.F.; Coderre, J.A.; Graça, M.; Vicente, H.; Blue, T.E. Boron Neutron Capture Therapy of Cancer: Current Status and Future Prospects. *Clin. Cancer Res.* **2005**, *11*, 3987–4002. [[CrossRef](#)]
10. Hopewell, J.W.; Morris, G.M.; Schwint, A.; Coderre, J.A. The Radiobiological Principles of Boron Neutron Capture Therapy: A Critical Review. *Appl. Radiat. Isot.* **2011**, *69*, 1756–1759. [[CrossRef](#)]
11. Dymova, M.A.; Taskaev, S.Y.; Richter, V.A.; Kuligina, E.V. Boron Neutron Capture Therapy: Current Status and Future Perspectives. *Cancer Commun.* **2020**, *40*, 406–421. [[CrossRef](#)]
12. Suzuki, M. Boron Neutron Capture Therapy (BNCT): A Unique Role in Radiotherapy with a View to Entering the Accelerator-Based BNCT Era. *Int. J. Clin. Oncol.* **2020**, *25*, 43–50. [[CrossRef](#)]
13. Coderre, J.A.; Morris, G.M. The Radiation Biology of Boron Neutron Capture Therapy. *Radiat. Res.* **1999**, *151*, 1–18. [[CrossRef](#)]
14. Skwierawska, D.; López-Valverde, J.A.; Balcerzyk, M.; Leal, A. Clinical Viability of Boron Neutron Capture Therapy for Personalized Radiation Treatment. *Cancers* **2022**, *14*, 2865. [[CrossRef](#)]
15. Schwint, A.E.; Monti Hughes, A.; Garabalino, M.A.; Pozzi, E.C.C.; Heber, E.M.; Trivillin, V.A. Translational Radiobiological Boron Neutron Capture Therapy (BNCT) Studies for the Treatment of Different Pathologies: A Bench to Bedside Approach. *Austin J. Nanomed. Nanotechnol.* **2018**, *6*, 1049.
16. Malouff, T.D.; Seneviratne, D.S.; Ebner, D.K.; Stross, W.C.; Waddle, M.R.; Trifiletti, D.M.; Krishnan, S. Boron Neutron Capture Therapy: A Review of Clinical Applications. *Front. Oncol.* **2021**, *11*, 601820. [[CrossRef](#)]
17. Wang, S.; Zhang, Z.; Miao, L.; Li, Y. Boron Neutron Capture Therapy: Current Status and Challenges. *Front. Oncol.* **2022**, *12*, 788770. [[CrossRef](#)]
18. Monti Hughes, A. Importance of Radiobiological Studies for the Advancement of Boron Neutron Capture Therapy (BNCT). *Expert Rev. Mol. Med.* **2022**, *24*, e14. [[CrossRef](#)]
19. Wang, P.; Zhen, H.; Jiang, X.; Zhang, W.; Cheng, X.; Guo, G.; Mao, X.; Zhang, X. Boron Neutron Capture Therapy Induces Apoptosis of Glioma Cells through Bcl-2/Bax. *BMC Cancer* **2010**, *10*, 661. [[CrossRef](#)]
20. Chen, K.H.; Lai, Z.Y.; Li, D.Y.; Lin, Y.C.; Chou, F.I.; Chuang, Y.J. Analysis of DNA Damage Responses after Boric Acid-Mediated Boron Neutron Capture Therapy in Hepatocellular Carcinoma. *Anticancer Res.* **2019**, *39*, 6661–6671. [[CrossRef](#)]
21. Ferrari, C.; Bakeine, J.; Ballarini, F.; Boninella, A.; Bortolussi, S.; Bruschi, P.; Cansolino, L.; Clerici, A.M.; Coppola, A.; Di Liberto, R.; et al. In Vitro and In Vivo Studies of Boron Neutron Capture Therapy: Boron Uptake/Washout and Cell Death. *Radiat. Res.* **2011**, *175*, 452–462. [[CrossRef](#)]
22. Okamoto, E.; Yamamoto, T.; Nakai, K.; Yoshida, F.; Matsumura, A. Detection of DNA Double-Strand Breaks in Boron Neutron Capture Reaction. *Appl. Radiat. Isot.* **2015**, *106*, 185–188. [[CrossRef](#)]
23. Fujita, Y.; Kato, I.; Iwai, S.; Ono, K.; Suzuki, M.; Sakurai, Y.; Ohnishi, K.; Yura, Y. Role of P53 Mutation in the Effect of Boron Neutron Capture Therapy on Oral Squamous Cell Carcinoma. *Radiat. Oncol.* **2009**, *4*, 63. [[CrossRef](#)]
24. Maliszewska-Olejniczak, K.; Kaniowski, D.; Araszkiwicz, M.; Tymińska, K.; Korgul, A. Molecular Mechanisms of Specific Cellular DNA Damage Response and Repair Induced by the Mixed Radiation Field During Boron Neutron Capture Therapy. *Front. Oncol.* **2021**, *11*, 676575. [[CrossRef](#)]
25. Kinashi, Y.; Takahashi, S.; Kashino, G.; Okayasu, R.; Masunaga, S.; Suzuki, M.; Ono, K. DNA Double-Strand Break Induction in Ku80-Deficient CHO Cells Following Boron Neutron Capture Reaction. *Radiat. Oncol.* **2011**, *6*, 106. [[CrossRef](#)]
26. Iliakis, G.; Mladenov, E.; Mladenova, V. Necessities in the Processing of DNA Double Strand Breaks and Their Effects on Genomic Instability and Cancer. *Cancers* **2019**, *11*, 1671. [[CrossRef](#)]
27. Georgakilas, A.G.; O'Neill, P.; Stewart, R.D. Induction and Repair of Clustered DNA Lesions: What Do We Know so Far? *Radiat. Res.* **2013**, *180*, 100–109. [[CrossRef](#)]
28. Hada, M.; Georgakilas, A.G. Formation of Clustered DNA Damage after High-LET Irradiation: A Review. *J. Radiat. Res.* **2008**, *49*, 203–210. [[CrossRef](#)]
29. Ballarini, F.; Bakeine, J.; Bortolussi, S.; Bruschi, P.; Cansolino, L.; Clerici, A.M.; Ferrari, C.; Protti, N.; Stella, S.; Zonta, A.; et al. Cell Death Following BNCT: A Theoretical Approach Based on Monte Carlo Simulations. *Appl. Radiat. Isot.* **2011**, *69*, 1745–1747. [[CrossRef](#)]

30. Anderson, R.M.; Marsden, S.J.; Wright, E.G.; Kadhim, M.A.; Goodhead, D.T.; Griffin, C.S. Complex Chromosome Aberrations in Peripheral Blood Lymphocytes as a Potential Biomarker of Exposure to High-LET α -Particles. *Int. J. Radiat. Biol.* **2000**, *76*, 31–42. [[CrossRef](#)]
31. Manti, L.; Durante, M.; Grossi, G.; Ortenzia, O.; Pugliese, M.; Scampoli, P.; Gialanella, G. Measurements of Metaphase and Interphase Chromosome Aberrations Transmitted through Early Cell Replication Rounds in Human Lymphocytes Exposed to Low-LET Protons and High-LET ¹²C Ions. *Mutat. Res.* **2006**, *596*, 151–165. [[CrossRef](#)]
32. Kawata, T.; Ito, H.; George, K.; Wu, H.; Cucinotta, F.A. Chromosome Aberrations Induced by High-LET Radiations. *Biol. Sci. Space* **2004**, *18*, 216–223. [[CrossRef](#)]
33. Savage, J.R.; Simpson, P.J. FISH “Painting” Patterns Resulting from Complex Exchanges. *Mutat. Res.* **1994**, *312*, 51–60. [[CrossRef](#)]
34. Cornforth, M.N. Analyzing Radiation-Induced Complex Chromosome Rearrangements by Combinatorial Painting. *Radiat. Res.* **2001**, *155*, 643–659. [[CrossRef](#)]
35. Anderson, R. Multiplex Fluorescence in Situ Hybridization (M-FISH). *Methods Mol. Biol.* **2010**, *659*, 83–97. [[CrossRef](#)]
36. Anderson, R.M.; Stevens, D.L.; Goodhead, D.T. M-FISH Analysis Shows That Complex Chromosome Aberrations Induced by Alpha-Particle Tracks Are Cumulative Products of Localized Rearrangements. *Proc. Natl. Acad. Sci. USA* **2002**, *99*, 12167–12172. [[CrossRef](#)]
37. Debnath, J.; Muthuswamy, S.K.; Brugge, J.S. Morphogenesis and Oncogenesis of MCF-10A Mammary Epithelial Acini Grown in Three-Dimensional Basement Membrane Cultures. *Methods* **2003**, *30*, 256–268. [[CrossRef](#)]
38. Bortolussi, S.; Protti, N.; Ferrari, M.; Postuma, I.; Fatemi, S.; Prata, M.; Ballarini, F.; Carante, M.P.; Farias, R.; González, S.J.; et al. Neutron flux and gamma dose measurement in the BNCT irradiation facility at the TRIGA reactor of the University of Pavia. *Nucl. Instrum. Methods Phys. Res. Sect. B* **2018**, *414*, 113–120. [[CrossRef](#)]
39. Viegas, A.M.D.; Postuma, I.; Bortolussi, S.; Guidi, C.; Riback, J.S.; Provenzano, L.; Marcaccio, B.; Rossini, A.E.; Ferrari, C.; Cansolino, L.; et al. Detailed Dosimetry Calculation for In-Vitro Experiments and Its Impact on Clinical BNCT. *Phys. Med.* **2021**, *89*, 282–292. [[CrossRef](#)]
40. Postuma, I.; Bortolussi, S.; Protti, N.; Ballarini, F.; Bruschi, P.; Ciani, L.; Ristori, S.; Panza, L.; Ferrari, C.; Cansolino, L.; et al. An Improved Neutron Autoradiography Set-up for ¹⁰B Concentration Measurements in Biological Samples. *Rep. Pract. Oncol. Radiother.* **2016**, *21*, 123–128. [[CrossRef](#)]
41. Manti, L.; Braselmann, H.; Calabrese, M.L.; Massa, R.; Pugliese, M.; Scampoli, P.; Sicignano, G.; Grossi, G. Effects of Modulated Microwave Radiation at Cellular Telephone Frequency (1.95 GHz) on X-ray-Induced Chromosome Aberrations in Human Lymphocytes in Vitro. *Radiat. Res.* **2008**, *169*, 575–583. [[CrossRef](#)]
42. Durante, M.; Furusawa, Y.; Gotoh, E. A Simple Method for Simultaneous Interphase-Metaphase Chromosome Analysis in Biodosimetry. *Int. J. Radiat. Biol.* **1998**, *74*, 457–462. [[CrossRef](#)]
43. Manti, L.; Durante, M.; Cirrone, G.A.P.; Grossi, G.; Lattuada, M.; Pugliese, M.; Sabini, M.G.; Scampoli, P.; Valastro, L.; Gialanella, G. Modelled Microgravity Does Not Modify the Yield of Chromosome Aberrations Induced by High-Energy Protons in Human Lymphocytes. *Int. J. Radiat. Biol.* **2005**, *81*, 147–155. [[CrossRef](#)]
44. Savage, J.R. Classification and Relationships of Induced Chromosomal Structural Changes. *J. Med. Genet.* **1976**, *13*, 103–122. [[CrossRef](#)]
45. Lee, R.; Sommer, S.; Hartel, C.; Nasonova, E.; Durante, M.; Ritter, S. Complex Exchanges Are Responsible for the Increased Effectiveness of C-Ions Compared to X-rays at the First Post-Irradiation Mitosis. *Mutat. Res.* **2010**, *701*, 52–59. [[CrossRef](#)]
46. Couto, M.; Alamón, C.; Nievas, S.; Perona, M.; Dargosa, M.A.; Teixidor, F.; Cabral, P.; Viñas, C.; Cerecetto, H. Bimodal Therapeutic Agents against Glioblastoma, One of the Most Lethal Forms of Cancer. *Chemistry* **2020**, *26*, 14335–14340. [[CrossRef](#)]
47. Schwint, A.E.; Garabalino, M.A.; Hughes, A.M.; Pozzi, E.C.C.; Heber, E.M.; Palmieri, M.A.; Trivillin, V.A. Teachings of Our Translational Studies on Boron Neutron Capture Therapy (BNCT): Thinking “Outside the Box”. *Ther. Radiol. Oncol.* **2019**, *3*, 20. [[CrossRef](#)]
48. Nikitaki, Z.; Velapoulou, A.; Zanni, V.; Tremi, I.; Havaki, S.; Kokkoris, M.; Gorgoulis, V.G.; Koumenis, C.; Georgakilas, A.G. Key Biological Mechanisms Involved in High-LET Radiation Therapies with a Focus on DNA Damage and Repair. *Expert Rev. Mol. Med.* **2022**, *24*, e15. [[CrossRef](#)]
49. Kawabata, S.; Suzuki, M.; Hirose, K.; Tanaka, H.; Kato, T.; Goto, H.; Narita, Y.; Miyatake, S.I. Accelerator-Based BNCT for Patients with Recurrent Glioblastoma: A Multicenter Phase II Study. *Neurooncol. Adv.* **2021**, *3*, vdab067. [[CrossRef](#)]
50. Rodriguez, C.; Carpano, M.; Curotto, P.; Thorp, S.; Casal, M.; Juvenal, G.; Pisarev, M.; Dargosa, M.A. In Vitro Studies of DNA Damage and Repair Mechanisms Induced by BNCT in a Poorly Differentiated Thyroid Carcinoma Cell Line. *Radiat. Environ. Biophys.* **2018**, *57*, 143–152. [[CrossRef](#)]
51. Schipler, A.; Iliakis, G. DNA Double-Strand-Break Complexity Levels and Their Possible Contributions to the Probability for Error-Prone Processing and Repair Pathway Choice. *Nucleic Acids Res.* **2013**, *41*, 7589–7605. [[CrossRef](#)]
52. Murmann-Konda, T.; Soni, A.; Stuschke, M.; Iliakis, G. Analysis of Chromatid-Break-Repair Detects a Homologous Recombination to Non-Homologous End-Joining Switch with Increasing Load of DNA Double-Strand Breaks. *Mutat. Res. Genet. Toxicol. Environ. Mutagen.* **2021**, *867*, 503372. [[CrossRef](#)]
53. Abbotts, R.; Wilson, D.M., 3rd. Coordination of DNA Single Strand Break Repair. *Free Radic. Biol. Med.* **2017**, *107*, 228–244. [[CrossRef](#)]
54. Mladenova, V.; Mladenov, E.; Chaudhary, S.; Stuschke, M.; Iliakis, G. The High Toxicity of DSB-Clusters Modelling High-LET-DNA Damage Derives from Inhibition of c-NHEJ and Promotion of Alt-EJ and SSA despite Increases in HR. *Front. Cell Dev. Biol.* **2022**, *10*, 1016951. [[CrossRef](#)]

55. Schmid, T.E.; Canella, L.; Kudejova, P.; Wagner, F.M.; Röhrmoser, A.; Schmid, E. The Effectiveness of the High-LET Radiations from the Boron Neutron Capture [$^{10}\text{B}(n,\alpha)^7\text{Li}$] Reaction Determined for Induction of Chromosome Aberrations and Apoptosis in Lymphocytes of Human Blood Samples. *Radiat. Environ. Biophys.* **2015**, *54*, 91–102. [[CrossRef](#)]
56. Ritter, S.; Nasonova, E.; Furusawa, Y.; Ando, K. Relationship between Aberration Yield and Mitotic Delay in Human Lymphocytes Exposed to 200 MeV/u Fe-Ions or X-rays. *J. Radiat. Res.* **2002**, *43*, S175–S179. [[CrossRef](#)]
57. Cornforth, M.N.; Bedford, J.S. A Quantitative Comparison of Potentially Lethal Damage Repair and the Rejoining of Interphase Chromosome Breaks in Low Passage Normal A Quantitative Comparison of Potentially Lethal Damage Repair and the Rejoining of Interphase Chromosome Breaks in Low Passage Normal Human Fibroblasts. *Radiat. Res.* **1987**, *111*, 385–405.
58. Konings, K.; Vandevoorde, C.; Baselet, B.; Baatout, S.; Moreels, M. Combination Therapy with Charged Particles and Molecular Targeting: A Promising Avenue to Overcome Radioresistance. *Front. Oncol.* **2020**, *10*, 128. [[CrossRef](#)]
59. Ricciardi, V.; Portaccio, M.; Piccolella, S.; Manti, L.; Pacifico, S.; Lepore, M. Study of SH-SY5Y Cancer Cell Response to Treatment with Polyphenol Extracts Using FT-IR Spectroscopy. *Biosensors* **2017**, *7*, 57. [[CrossRef](#)]
60. Cirrone, G.A.P.; Margarone, D.; Maggiore, M.; Anzalone, A.; Borghesi, M.; Jia, S.B.; Bulanov, S.S.; Bulanov, S.; Carpinelli, M.; Cavallaro, S.; et al. ELIMED: A new hadron therapy concept based on laser driven ion beams. In Proceedings of the SPIE, The International Society for Optical Engineering, Prague, Czech Republic, 15–18 April 2013; Volume 8779. [[CrossRef](#)]
61. Ban, H.S.; Nakamura, H. Boron-Based Drug Design. *Chem. Rec.* **2015**, *15*, 616–635. [[CrossRef](#)]
62. Nuez-Martinez, M.; Pinto, C.I.G.; Guerreiro, J.F.; Mendes, F.; Marques, F.; Muñoz-Juan, A.; Xavier, J.A.M.; Laromaine, A.; Bitonto, V.; Protti, N.; et al. Cobaltabis(Dicarbollide) ([o-Cosan][−]) as Multifunctional Chemotherapeutics: A Prospective Application in Boron Neutron Capture Therapy (BNCT) for Glioblastoma. *Cancers* **2021**, *13*, 6367. [[CrossRef](#)]
63. Matsumura, A.; Asano, T.; Hirose, K.; Igaki, H.; Kawabata, S.; Kumada, H. Initiatives Toward Clinical Boron Neutron Capture Therapy in Japan. *Cancer Biother. Radiopharm.* **2023**, *38*, 201–207. [[CrossRef](#)]

Disclaimer/Publisher’s Note: The statements, opinions and data contained in all publications are solely those of the individual author(s) and contributor(s) and not of MDPI and/or the editor(s). MDPI and/or the editor(s) disclaim responsibility for any injury to people or property resulting from any ideas, methods, instructions or products referred to in the content.